ACS APPLIED MATERIALS & INTERFACES

Research Article

www.acsami.org

Investigation of the Interfacial Effects of Small Chemical-Modified TiO_2 Nanotubes on 3T3 Fibroblast Responses

Shu-Ping Lin,*[,†,‡] Shu-Yen Huang,[†] Se-Fen Chen,[†] Lester U. Vinzons,[†] Jhong-Yi Ciou,[§] and Pei-Jie Wong[§]

[†]Graduate Institute of Biomedical Engineering, [§]Bachelor Program of Biotechnology, National Chung Hsing University, 250 Kuo-Kuang Road, Taichung, 40227 Taiwan

[‡]Biomedical Engineering and System Bioinformatics Research Center, Kaohsiung Medical University, Kaohsiung, Taiwan

Supporting Information

ABSTRACT: In order to gain insight into how interfacial effects influence cell responses, chemically modified anodized TiO_2 nanotubes (ATNs) were used to simultaneously investigate the effects of nanoscale substrate structure and angstrom-scale chemicals on cell morphological change and cell growth. Two small chemicals were used to modify the ATNs, namely, 3-aminopropyltrimethoxysilane (APTMS) and 3-mercaptopropyltrimethoxysilane (MPTMS), resulting in APTMS-modified ATNs (APTMS-ATNs) and MPTMS-modified ATNs (MPTMS-ATNs), respectively. In our *in vitro* observation of NIH/3T3 fibroblasts, cells thrived on both unmodified and modified ATNs. Quantitative analyses of cell numbers exhibited that APTMS-ATNs effectively facilitated cell proliferation and directed cell orientation owing to full cell−substrate contact caused by positively charged amino groups ($-NH_3^+$) on the surface. In addition, scanning electron microscopy and fluorescence images showed different cell morphologies on APTMS-ATNs and MPTMS-ATNs. APTMS-ATNs resulted in flat spreading of fibroblasts, while MPTMS-ATNs resulted in fibroblasts with a three-dimensional solid shape and clear contours. The results indicate that the synergistic effects of nanotube surface topology and small chemical modification and, to a lesser extent, surface hydrophilicity, alter the interfacial interactions between cells and substrates, significantly affecting cell morphology, attachment, and growth. Using ATNs with different interfacial effects from various small chemicals, orientation of cells into various patterns can be achieved and investigation of cell fates, such as proliferation or stem cell differentiation, can be performed for future advanced medical or biological applications.

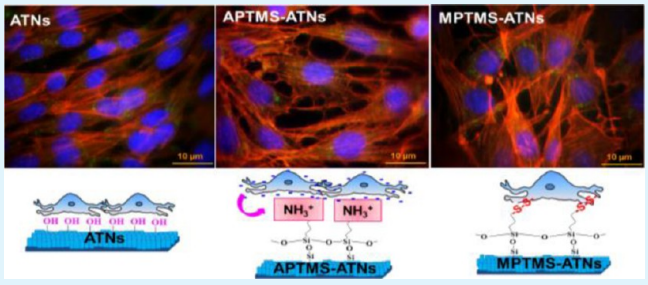

KEYWORDS: *TiO_2, nanotubes, surface modification, functional groups, interfacial effect, cell response*

INTRODUCTION

Understanding cell−substrate interaction is a prerequisite for the effective control of the function, growth, and movement of cells in both *in vitro* and *in vivo* environments. The interplay between cells and the underlying substrate also gives an insight into cell fate and thus determines the criteria for the design of biocompatible materials. Recently, a number of studies have been conducted on the interaction between cells and biomaterials with micro- or submicroscale to nanoscale features.[1−9] Due to the size scale of the subcellular structures, such as integrins, on the membrane of mammalian cells, investigation of cell responses in the nanoscale regime will not only predict cell behavior during proliferation or differentiation but also enable the development of materials truly compatible with the biological system.

In order to determine how cells respond to minute structural changes in the substrate, nanostructures based on existing micro- and submicro-architectures have been fabricated using various techniques, such as nanoelectromechanical system techniques for creating nanogrooves,[10] nanopits,[11] or nanopillars;[2] vapor−liquid−solid process for growing nanowires;[12,13] chemical vapor deposition for forming nanotubes;[8,14] acid etching for constructing nanonodules;[9,15] colloidal synthesis of nanoparticles;[16] polymer demixing for generating nanoislands;[17,18] and electrochemical anodization for fabricating nanotubes[7,19] or nanopillars.[20] The primary considerations in the creation of these nanodimensional structures have been the cost of fabrication and the uniformity and uniqueness of the architecture. Among the various techniques employed so far, electrochemical anodization is one of the most prevalent, especially for the creation of various sizes of nanotubular architectures on certain metals,[21] such as aluminum[22] and titanium.[21] The nanotubular structures offer the advantage of having random nanoparticles replaced by highly ordered tubes. Furthermore, the nanotubular structures increase the surface

Received: February 21, 2014
Accepted: July 11, 2014
Published: July 11, 2014

roughness of the substrate and have a well-defined and controllable pore size, wall thickness, and tube length.[23]

The nanoscale topography of material surfaces has been reported to affect cell activities.[1] Previous studies indicate that nanostructures significantly influence different cell features and behavior, such as morphology, extension, migration, growth, differentiation, protrusion of filopodia, and cell proliferation.[2−10,12,19,21,24−28] For example, nanotopographical groove structures with a depth of 85−100 nm were shown to have a great impact on fibroblast growth during regeneration of the periodontal ligament.[10] Moreover, TiO_2 nanotubes having diameters larger than 50 nm resulted in dramatically reduced cell adhesion and spreading and a high extent of programmed cell death among mesenchymal stem cells (MSCs).[7] On the other hand, TiO_2 nanotubes 15 nm in diameter were found to influence MSCs differentiation by inducing osteoclastic activation and bone-forming activity.[19] Similarly, 300 nm nanonodules hybridized with micropits enhanced differentiation and proliferation of bone marrow-derived osteoblasts.[9] Among these studies, there is still disagreement over how the topography and dimensions of nanostructures particularly affect cell fate. Furthermore, the above-mentioned nanostructures had been chemically modified or physically coated with biomolecules of limited shelf life prior to biological and medical applications. There is currently a lack of studies on the feasibility of using small chemicals to substitute for commonly used biomolecules and the influence of such chemicals on cell fate, such as cell cycle phase during proliferation and changes in cell morphology during differentiation.

In this study, we propose a method for investigating the interfacial effects of small chemicals on cell responses using chemically modified, anodized TiO_2 nanotubes (ATNs). ATNs were fabricated in sodium fluoride, sulfuric acid, and ethylene glycol containing electrolyte. The ATNs were treated with oxygen plasma and modified with either 3-aminopropyltrimethoxysilane (APTMS) or 3-mercaptopropyltrimethoxysilane (MPTMS), resulting in APTMS-modified ATNs (APTMS-ATNs) and MPTMS-modified ATNs (MPTMS-ATNs), respectively. These ATNs were then utilized to observe the interfacial effects of chemically modified nanostructures on the morphology, growth, viability, and proliferation of cells using NIH/3T3 fibroblasts, one of the most common cells in connective tissues. In this study, we also discuss how the small chemical-modified ATNs affect the cell cycle phase and the number and length of filopodia of fibroblast cells.

EXPERIMENTAL SECTION

Fabrication of ATNs. Titanium webs (99.9% purity, 3 mm nominal aperture, 0.35 mm wire diameter, 51% open rate, Shang Kai Steel Co., Ltd.) were degreased by sonication in acetone, 10% hydrochloric acid (HCl, J.T. Baker), isopropanol, and methanol, followed by rinsing with deionized (DI) water and drying in a nitrogen stream prior to anodization. A two-electrode electrochemical anodization cell, with a platinum electrode as the cathode and the Ti web as the anode positioned in parallel 5 cm apart, was used to fabricate TiO_2 nanotubes. Anodization was performed at a constant voltage of 20 V using a DC power supply (GPC-3020D, GW Instek) and with continuous mixing by a magnetic stirrer at 60 °C for 20 min. The hydrofluoric acid (HF)-free electrolyte contained 0.1 M sodium fluoride (NaF, Sigma), 1 M sulfuric acid (H_2SO_4, J.T. Baker), and 5% ethylene glycol ($C_2H_4(OH)_2$, J.T. Baker) in DI water at pH 4. The resulting ATNs were rinsed several times with DI water and dried in the air. After drying, residues on the surfaces of the ATNs were removed by sonication in acetone for 3 min. ATN samples were then annealed at 400 °C for 3 h in nitrogen gas. Finally, ATN samples were cleaned by oxygen plasma for 10 s to remove organic contaminants.

Surface Modification of ATNs. ATN samples were modified with 1% ethanolic solutions of the chemicals APTMS ($H_2N(CH_2)_3Si(OCH_3)_3$, Sigma) and MPTMS ($HS-(CH_2)_3Si(OCH_3)_3$, Sigma) for 2 h to provide amine and mercapto functional groups, respectively, to the ATN surfaces. After functionalization, the APTMS-ATNs and MPTMS-ATNs were separately rinsed with ethanol several times and then heated in ethanol in an oven at 60 °C for 5 min. All samples were dried in a nitrogen stream.

Characterization of Materials. The Ti web, ATN, APTMS-ATN, and MPTMS-ATN samples were characterized by electron spectroscopy for chemical analysis (ESCA) for surface characterization of materials and by nanodrop contact angle measurement for evaluation of nanoscale surface properties.

The characteristic elemental compositions and chemical structures of the material surfaces were examined by ESCA. The ESCA spectra were acquired with Microlab 310F (VG Scientific) and nonmonochromatic magnesium anode X-ray at 400 W, 15 kV, and 10 mA (Kα 1253.6 eV, a concentric hemispherical capacitor analyzer). In the quantitative determination of the elemental compositions, the Ti_{2p}, O_{1s}, C_{1s}, N_{1s}, $S_{2p3/2}$ and Si_{2p} core level spectra were measured and calculated from the ESCA peak area with correction algorithms and relative sensitivity factors.[29] The compositional peaks of N_{1s} and $S_{2p3/2}$ were identified using the XPS Peak fitting program and a Shirley background,[30] together with a database for elements and native oxides[31] and organic polymers.[32]

The nanoscale surface property was evaluated via the sessile drop method using a computer-automated goniometer (OCA20, Dataphysics). The water contact angles were measured and averaged using six nanoliter-drops (i.e., each drop with a volume of 1 μL).

NIH/3T3 Fibroblast Culture. The Ti web, ATN, APTMS-ATN, and MPTMS-ATN samples used for the cell culture assays were first cleaned by immersing in 70% ethanol solution overnight and irradiating with ultraviolet light for 30 min. The samples were then washed with sterile phosphate buffered saline (PBS) solution three times before cell seeding. NIH/3T3 fibroblasts (ATCC CRL-1658) were seeded on Ti web, ATN, APTMS-ATN, and MPTMS-ATN samples at a density of 5×10^5 cells/mL. The fibroblast cells were cultured in Dulbecco's modified Eagle's medium with 10% fetal bovine serum and 100 μg/mL penicillin−streptomycin in a humidified atmosphere with 5% CO_2 and 95% air at 37 °C. Cell culture media and supplements were purchased from Life Technologies.

Cell Growth Assay and Observation of Cell Morphology. Viability of cells cultured on Ti web, ATN, APTMS-ATN, and MPTMS-ATN samples was assessed using the LIVE/DEAD Viability/Cytotoxicity kit (Molecular Probes), which is capable of simultaneous determination of live and dead cells. Fluorescence observation of the LIVE/DEAD assay was performed separately for green and red emission (calcein AM and EthD-1, respectively) using a fluorescence microscope. Samples containing fibroblast cells were first washed by PBS to remove the nonadhered cells. Working solutions of calcein AM (2 μM) and EthD-1 (1 μM), for distinguishing live and dead cells, respectively, were added to the samples and incubated for

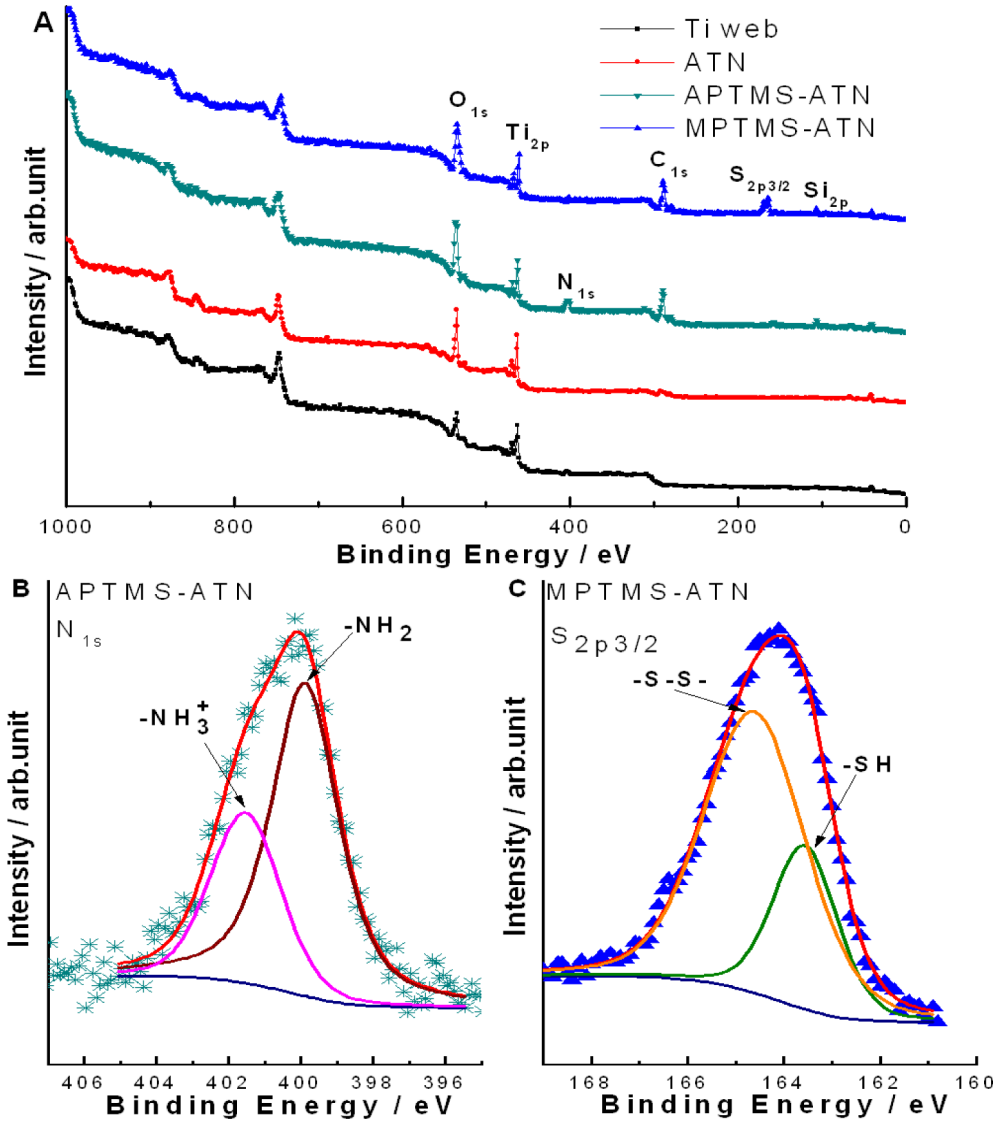

Figure 1. Chemical characterization of Ti web, ATN, APTMS-ATN, and MPTMS-ATN surfaces using ESCA. (A) The survey spectra reveal the atomic compositions of the samples. The spectra show that the porous layer of our ATNs consists of oxygen and titanium without any fluorine ions owing to the HF-free electrolyte. The characteristic elements of carbon and silicon appeared after the modification of ATNs with APTMS and MPTMS. Likewise, the characteristic elements of nitrogen and sulfur can be observed for APTMS-ATNs and MPTMS-ATNs, respectively. (B) Peaks for the amine functional group ($-NH_2$) and ammonium ion ($-NH_3^+$) were resolved at 399.9 and 401.5 eV, respectively, in the N_{1s} scan of the APTMS-ATN surface. (C) Peaks for the mercapto group (−SH) and disulfide bond (−S−S−) were resolved at 163.6 and 164.6 eV, respectively, in the $S_{2p3/2}$ scan of the MPTMS-ATN surface.

30 min. Six samples each for Ti web, ATN, APTMS-ATN, and MPTMS-ATN were used for the assessment of cell viability using image analysis software ImageJ (NIH, Bethesda, ML). Cell growth calculations were performed on each sample by enumerating the number of live cells per high-power field from captured digital images taken from six random fields.

In order to prepare cells for fluorescence observation of cell morphology, fibroblast cells were fixed on day 5 of culture with 4% paraformaldehyde for 20 min at RT. The fixed cells were then washed with PBS and treated with 0.1% Triton X-100 (American Bioanalytical). Samples were stained with 1 mg/mL DAPI and rhodamine−phalloidin (1:500, Molecular Probes) in PBS for 1 h. Afterward, cells were immunochemically stained with mouse antivinculin monocolonal antibody (1:200, Millipore), followed by FITC-conjugated antimouse secondary antibody (1:200, Millipore). Samples were washed twice with 1% bovine serum albumin in PBS and examined under a fluorescence microscope. Cell numbers and cell cycle phase for cell growth assay were determined using image analysis software MetaMorph (Molecular Devices) by enumerating the number DAPI-stained nuclei per high power field from captured digital images taken from six random fields.

Fluorescence observation and image capture of stained fibroblast cells were performed using a phase-contrast upright microscope (Eclipse 80i, Nikon) equipped with fluorescent optics and an intensified charged coupled device camera (Evolution VF, MediaCybernetics).

In order to confirm the cell growth measurements by the calcein AM (LIVE/DEAD) and DAPI staining, a colorimetric assay based on WST-1 (ab155902, Abcam) was used to measure cell proliferation in each sample. Samples were treated with WST-1 for 2 h in an incubator, and then the absorbance of the liquid from the samples was measured using UV−vis spectroscopy (Cintra 202, GBC) at 420−480 nm.

Table 1. Quantitative Determination of the Elemental Composition of Ti Web, ATN, APTMS-ATN, and MPTMS-ATN Surfaces Based on ESCA[a]

	atomic composition (%)					
	Ti_{2p}	O_{1s}	C_{1s}	N_{1s}	Si_{2p}	$S_{2p3/2}$
Ti web	61.79 ± 0.14	38.21 ± 0.14	–	–	–	–
ATN	34.98 ± 0.09	65.02 ± 0.09	–	–	–	–
APTMS-ATN	15.68 ± 0.07	68.58 ± 0.12	11.84 ± 0.07	2.59 ± 0.06	1.31 ± 0.11	–
MPTMS-ATN	15.91 ± 0.07	67.70 ± 0.08	12.34 ± 0.08	–	1.31 ± 0.10	2.73 ± 0.08

[a] $n = 9$; value (%) = mean ± SEM.

The morphology of the adhered cells on Ti webs, ATNs, APTMS-ATNs, and MPTMS-ATNs was also observed using scanning electron microscopy (SEM). After 5 days of culture, the samples were fixed in the 2.5% glutaraldehyde for 30 min, dehydrated in a graded series of ethanol, and washed three times for 15 min by absolute ethanol. The prepared samples were coated with a thin layer of gold using a sputter coater (Auto 108, Cressington) and then observed using SEM (JSM-6700F, JEOL). SEM images were thresholded to convert to binary images. And then, the evaluation of cell morphological change with regard to the total number and length of filopodia per cell was performed using ImageJ. The means and standard errors of cell morphological change were statistically analyzed. Thirty cells were selected randomly for evaluation. Cells that were clustered together were excluded in the analyses of filopodia expression among the fibroblast cells.

Statistical Analyses. Contact angle data were analyzed for statistical significance using one-way analysis of variance (ANOVA) with Bonferroni's test (significance assessed at $p < 0.05$). Cell morphological change and cell growth data were analyzed for statistical significance using one-way ANOVA with Tukey's pairwise comparisons test (significance assessed at $p < 0.05$).

RESULTS AND DISCUSSION

Characterization of Small Chemicals. Before the investigation of interfacial effects on cell responses, unmodified and modified ATN structures were characterized and analyzed by ESCA and contact-angle measurements to look for possible factors in the small chemical modifications affecting cell fates.

Figure 1A shows the survey spectrum from the ESCA analyses of Ti web, ATN, APTMS-ATN and MPTMS-ATN samples. The quantitative atomic compositions of the samples are listed in Table 1. Figure S1 (in Supporting Information [SI]) shows that our ATN fabrication process successfully created nanotubular TiO_2 structures on the Ti web. ESCA analyses revealed that the nanotube layer of our ATNs with pores 60 nm in diameter (Figure S1B–D in SI) consisted of approximately 65% oxygen and 35% titanium. The lack of any observable change in the macro- and nanoscales among plasma-cleaned ATNs, APTMS-ATNs, and MPTMS-ATNs (Figure S1B–D in SI) is expected. Plasma cleaning with O_2 gas only breaks organic bonds of surface contaminants, resulting in an ultraclean surface; it does not result in any physical or chemical change in the ATN material. On the other hand, APTMS and MPTMS are molecules with a length of ~0.8 nm, which is too small to be viewed by the SEM equipment used. In addition, the surface modification time was only limited to 1 h; therefore, the resulting APTMS and MPTMS modification would most probably be a monolayer, which has a thickness of a single APTMS or MPTMS molecule.

The ESCA and X-ray diffraction (XRD) results (Figure S1E,F in SI) clearly show that our ATNs consisted of TiO_2 and were free of fluorine ions owing to the HF-free electrolyte unlike in other studies.[7,33] ATNs with a high degree of biocompatibility are required for biomedical applications, such as in dental[10,34] or bone implants.[35] However, most reported ATN structures were fabricated in electrolytes containing HF.[7,19,36,37] Since fluorosis is widely known to cause cell death and decalcification of bones,[38] for medical applications, it is imprudent to utilize such ATN materials, which might contain remaining fluoride.

The characteristic elements of carbon and silicon in the molecules of APTMS and MPTMS appeared in the ESCA survey spectra after the chemical modification of ATNs, as can be seen in Figure 1A and Table 1. The characteristic peaks of nitrogen for APTMS and sulfur for MPTMS also appeared for APTMS-ATN and MPTMS-ATN samples, respectively, as shown in Figure 1A. Moreover, peaks for the amine functional group ($-NH_2$) and ammonium ion ($-NH_3^+$) were resolved at 399.9 and 401.5 eV, respectively, in the N_{1s} scan of the APTMS-ATN surface (Figure 1B). On the other hand, peaks for the mercapto group (−SH) and disulfide bond (−S−S−) were resolved at 163.6 and 164.6 eV, respectively, in the $S_{2p3/2}$ scan of the MPTMS-ATN surface (Figure 1C).

In terms of contact angle measurements, it was found that ATNs (51.13 ± 2.12°), APTMS-ATNs (42.85 ± 1.30°), and MPTMS-ATNs (61.98 ± 0.85°) were hydrophilic because they resulted in an average water contact angle significantly less than 90° (Figure 2).[39] On the other hand, Ti web is relatively hydrophobic because of a higher average water contact angle (87.08 ± 1.74°). The different degrees of hydrophilicity or hydrophobicity of materials are due to their varied surface properties, such as heterogeneity of the surface, produced by different treatments.

After anodization and plasma cleaning, contact angle measurements revealed that our ATNs became more hydrophilic (lower water contact angle) because of increased surface roughness and hydroxylation. Anodization of titanium substrates increases surface roughness and changes the chemical surface species, thereby altering the hydrophilicity of ATNs.[40] Oxygen-plasma cleaning after anodization can remove organic contaminants and increase oxygen-containing groups, such as −OH groups, to promote surface hydroxylation and further enhance wettability on our ATNs.[40−42] According to the ESCA N_{1s} scan of APTMS-ATNs, amine groups ($-NH_2$) have a tendency to ionize upon contact with water molecules, resulting in ammonium ions ($-NH_3^+$). These ammonium ions lead to ion−dipole attractive forces between APTMS molecules and water molecules, thereby resulting in the increased hydrophilicity of APTMS-ATNs. Even though APTMS molecules replace −OH groups on ATNs, the strength of an ion−dipole force is stronger than a dipole−dipole force or hydrogen

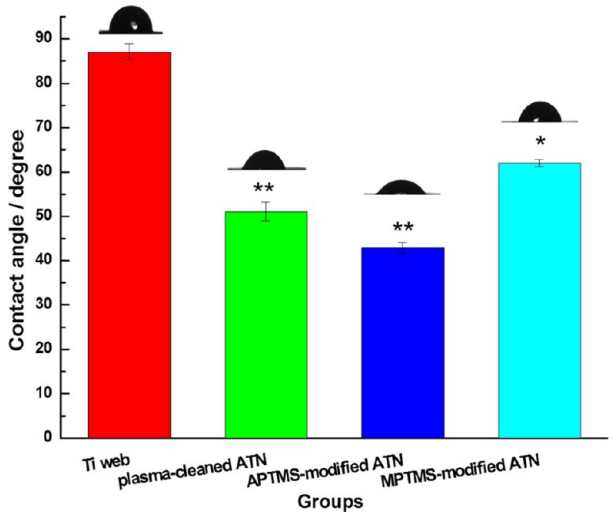

Figure 2. Evaluation of surface property of Ti web, ATN, APTMS-ATN, and MPTMS-ATN using contact angle measurements. Results show the degree of hydrophilicity/hydrophobicity of the samples: Ti web (87.08 ± 1.74°), ATN (51.13 ± 2.12°), APTMS-ATN (42.85 ± 1.30°), and MPTMS-ATN (61.98 ± 0.85°). $n = 6$; contact angle (deg) = mean ± SEM, $*p < 0.05$, $**p < 0.01$, significant difference relative to Ti web.

bonding.[43] Therefore, the net result is APTMS-ATNs having greater hydrophilicity than ATNs. On the other hand, MPTMS-ATNs were relatively hydrophobic in comparison with ATNs and APTMS-ATNs because of the hydrophobic property of the sulfur atom.[44]

Interfacial Effect of Small Chemicals on Cell Growth. ATNs with nanoscale tubular structures modified with small chemicals were fabricated to investigate the interfacial effects of angstrom-scale chemicals on the growth of fibroblasts, the most common cell in connective tissues. Cell viability is defined here as the number of fibroblasts that remain attached on the substrates (ATNs, APTMS-ATNs, and MPTMS-ATNs) after 5 days of culture. Images A–C of Figure 3 show the DAPI-stained nuclei of cells cultured on ATN, APTMS-ATN, and MPTMS-ATN samples, respectively.

Figure S2 (in SI) shows the results of cell cycle analyses of the fibroblast DNA labeled with DAPI using MetaMorph software. As shown in Table 2, the highest number of attached fibroblasts on day 5 was found on APTMS-ATNs, followed by MPTMS-ATNs, ATNs, and then raw Ti webs. Fibroblast cells cultured on a polystyrene dish served as the negative control. Cell growth in each sample was quantified by the total cell number on a 1 mm^2 area under different stages of the cell cycle, as determined by MetaMorph. Results of cell viability evaluation in the different samples indicate that Ti web has inherent biocompatibility in comparison with the dish. Statistical results of cell quantification using MetaMorph (Table 2) are 266.22 ± 5.34, 420.11 ± 8.68, and 353.22 ± 8.04 for ATN, APTMS-ATN, and MPTMS-ATN, respectively.

In order to verify the results of cell quantification using MetaMorph, *in situ* direct observation of cell viability on substrates was performed using LIVE/DEAD staining before cell fixation, followed by evaluation of cell viability using ImageJ. In Figure 3D–F, *in situ* LIVE/DEAD staining exhibits cell growth and viability on ATNs, APTMS-ATNs, and MPTMS-ATNs. On the basis of the occurrence of green fluorescence, cells thrived on all the ATNs samples. For each group of samples the results of cell growth, based on MetaMorph, were in accordance with the evaluation of viability/cytotoxicity using ImageJ (Table 2). Moreover, statistical results of cell viability using either MetaMorph or ImageJ are consistent with the results obtained using WST-1 assay, one of the common colorimetric assays used in the quantification of cell growth (Table 2). It is worthy to note that software analysis provides an alternative and convenient way to determine cell viability.

Cell cycle describes the sequence of activities a cell undergoes during proliferation, which involves a first checkpoint for DNA synthesis (G1), DNA replication (S), a second checkpoint signaling the start of cell division (G2), cell division (M), and finally the production of two daughter cells. Results of cell cycle analyses show that fibroblasts proliferated better on unmodified and modified ATN surfaces in comparison with culture dish and Ti web (Figure 3G). Cell numbers at G1, S, and late M phases significantly increased after 5 days of culture on APTMS-ATN and MPTMS-ATN. The results indicate that angstrom-scale chemicals, such as APTMS and MPTMS, on a nanoscale architecture considerably enhance cell growth and entry to specific phases of the cell cycle.

Apart from the surface topology of the ATN materials, the effect of enhanced hydrophilicity as a result of plasma cleaning and chemical surface modification on fibroblast attachment and growth was also explored. The dependence of cell spreading on surface energy, hydrophobicity, or hydrophilicity is not yet established because of contradicting observations on various bulk materials.[45−48] In this study, no significant difference was observed for relatively hydrophobic Ti web and hydrophilic dish in our cell growth observation (Table 2), suggesting minor influence of surface energy on cell attachment. On the other hand, the nanotubular surface of anodized TiO_2 has been used in many studies to investigate the feasibility of using those substrates as coatings for bone[25,28,49,50] and dental[10,15] implants. It has been shown that anodized TiO_2 surfaces provide a favorable substrate for growth and maintenance of bone cells.[49] *In vivo* rat studies showed that anodized TiO_2 is biocompatible, i.e., it does not cause chronic inflammation.[49] Furthermore, reduced bacterial adhesion and enhanced osteoblast differentiation have been observed on antibiotic-loaded TiO_2 nanotubes.[50]

It can be seen from Table 2 that there is a significant difference in the number of cells between all ATN materials and raw Ti web. This indicates that anodization imparts the Ti web with nanoscale structures favorable for cell attachment. The relatively higher cell number on all ATN surfaces compared with raw Ti web is primarily due to the rougher surface and greater surface area. This surface topology promotes a locked-in cell configuration, which enhances cell attachment and proliferation.[51] A previous study showed the ATNs provided accelerated cell–surface interaction and strongly enhanced cell activities.[51] Accordingly, all of our unmodified and modified nanoscale ATN structures are conducive to cell attachment and proliferation. Because of the unclear relationship between hydrophilicity and cell attachment, it is more likely that the nanostructures of the ATN surfaces have a more significant effect on cell adhesion than hydrophilicity. Moreover, APTMS modification resulted in an improvement of cell attachment, and, to some extent, cell proliferation, as can be seen in the 7-day culture in Figure S3 (in SI).

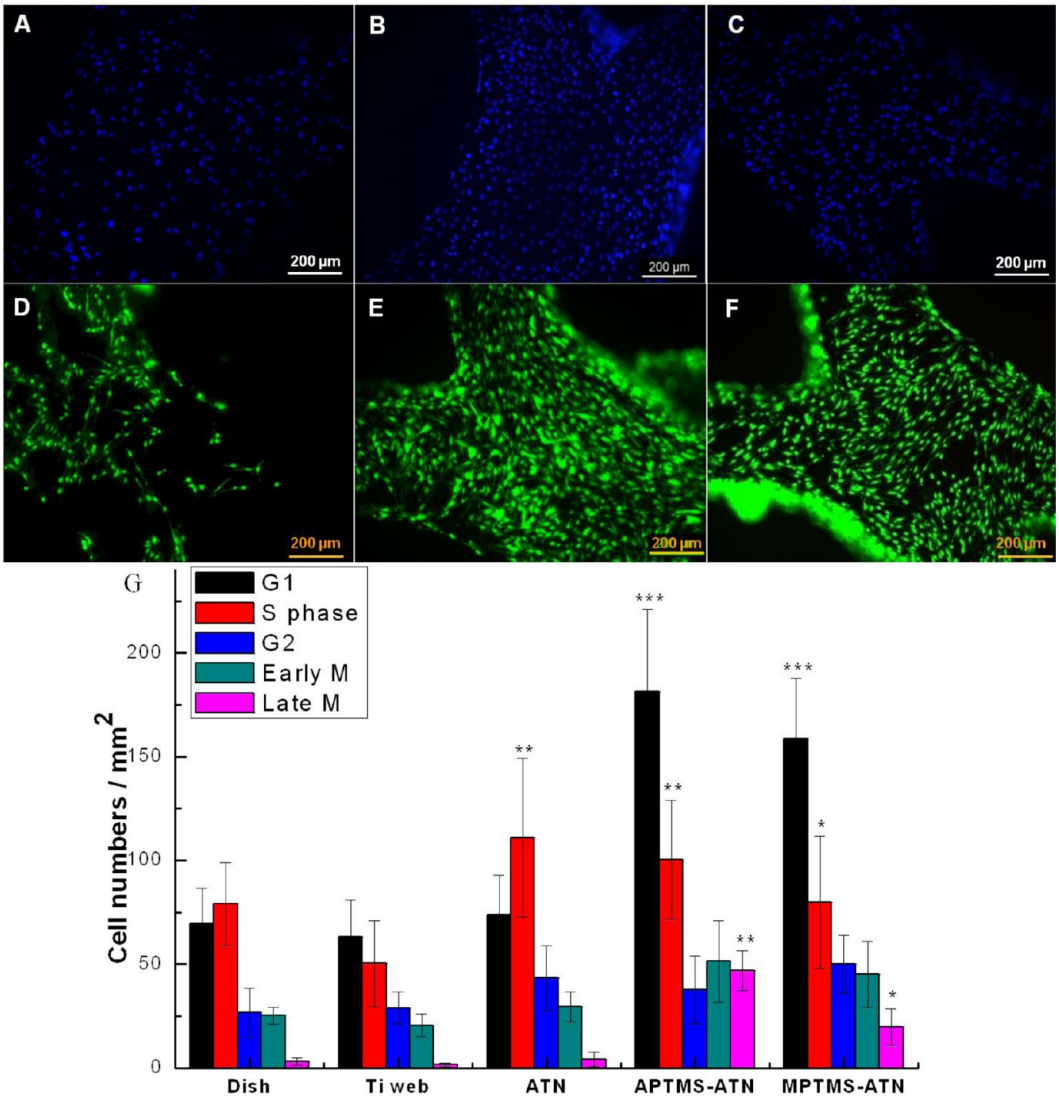

Figure 3. Cell viability of fibroblasts on various substrates after 5 days of culture. Fluorescence images show DAPI-stained nuclei of cells on ATN (A), APTMS-ATN (B), and MPTMS-ATN (C) and LIVE/DEAD-stained cells on ATN (D), APTMS-ATN (E), and MPTMS-ATN (F). The LIVE/DEAD staining demonstrates *in situ* cell growth and viability on the samples, as evaluated by ImageJ. (G) Results of statistical analyses of DAPI-stained nuclei on various substrates using MetaMorph showing cell numbers for different phases of the cell cycle. $n = 6$; value (cell number/mm^2) = mean ± SEM, *$p < 0.05$, **$p < 0.01$, ***$p < 0.001$, significant difference relative to Ti web. (See Figure S2 in SI for the detailed results of cell growth evaluation using MetaMorph for one trial.).

Table 2. Analyses[a] of Cell Viability in Ti web, ATN, APTMS-ATN, and MPTMS-ATN after 5 Days of Culture

	total cell number using MetaMorph cell cycle analysis	total cell number using ImageJ (LIVE/DEAD assay)	total cell number using WST-1 assay
polystyrene dish (negative control)	219.56 ± 5.68	244.56 ± 8.93	224.88 ± 3.92
Ti web	174.44 ± 5.24	197.56 ± 11.07	172.79 ± 6.42
ATN	266.22 ± 5.34 ([b])	285.44 ± 8.68 ([b])	258.16 ± 7.74 ([b])
APTMS-ATN	420.11 ± 8.68 ([c])	434.89 ± 11.80 ([c])	422.07 ± 5.90 ([c])
MPTMS-ATN	353.22 ± 8.04 ([c])	374.89 ± 10.52 ([c])	341.57 ± 6.34([c])

[a] $n = 9$; value (cell number/mm^2) = mean ± SEM. [b] $p < 0.05$. [c] $p < 0.01$, significant difference relative to Ti web.

Extracelluar matrix components, such as laminin, collagen, and fibronectin, have been utilized as biochemical cues to mediate the crosstalk between cells and materials and provide a suitable environment for cell attachment, differentiation, or proliferation.[1] Physical coating of substrates by such proteins has been widely used in conventional culture because the proteins are relatively easy to manipulate. However, protein coatings are likely to dissolve in static or dynamic culture conditions and easily lose their biofunctional and active properties. Therefore, it is advisable to search for suitable chemical molecules that can afford a long-term biocompatible and stable environment for cell growth. Furthermore, covalent immobilization of small chemicals on substrates can provide more resistance to harsh environments. From our results, the

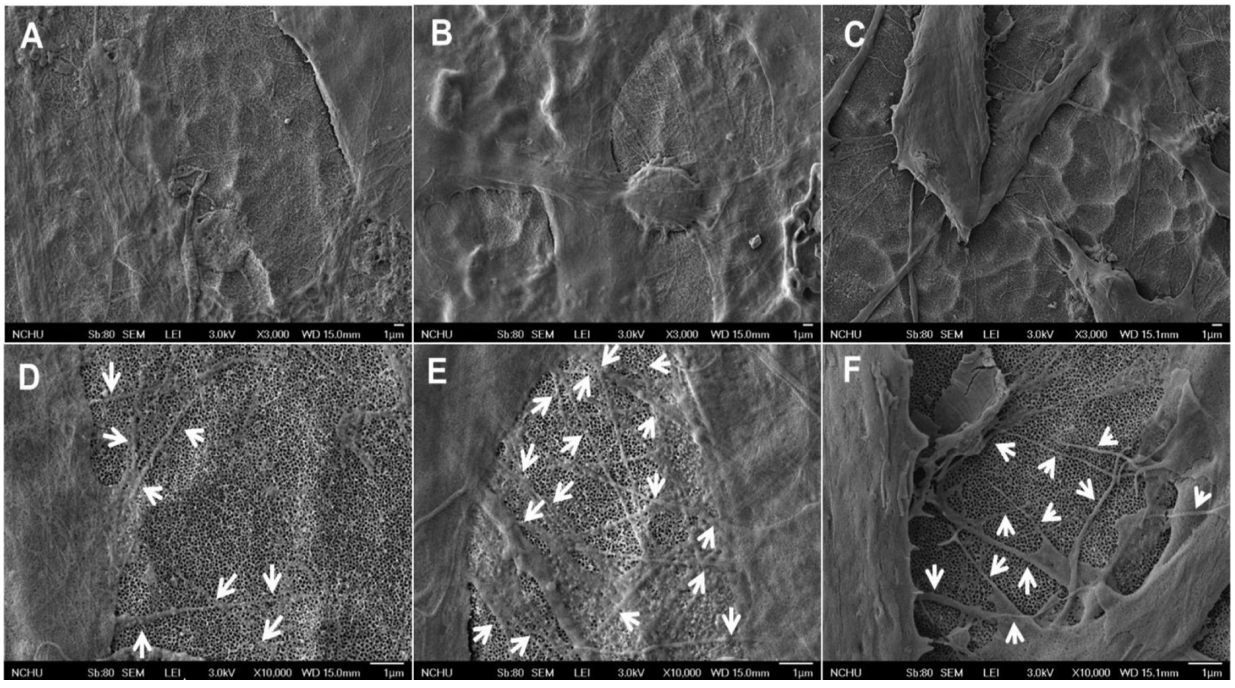

Figure 4. Representative SEM images of fibroblasts on unmodified and modified ATNs. Low-magnification images show the morphology of fibroblasts on ATN (A), APTMS-ATN (B), and MPTMS-ATN (C). High-magnification images of fibroblasts on ATN (D), APTMS-ATN (E), and MPTMS-ATN (F) corresponding to images (A), (B), and (C). The filopodia protrusions (white arrows) and cell morphology show different cell attachment behaviors on the various substrates.

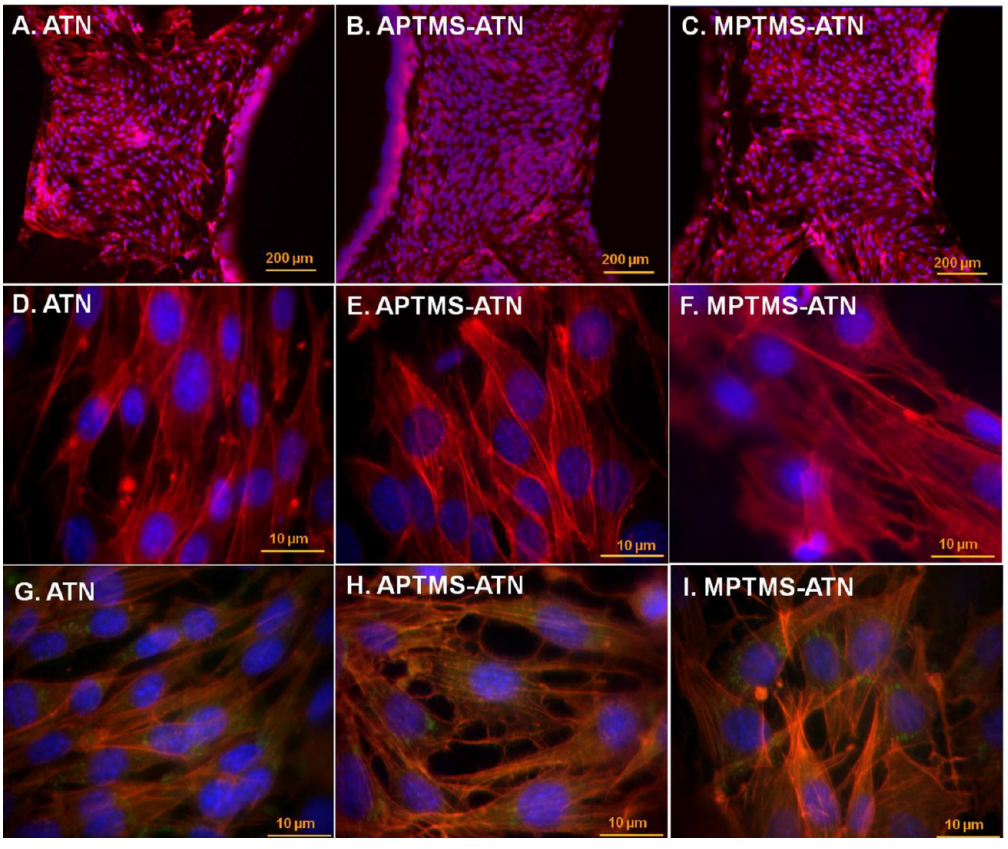

Figure 5. Fluorescence observation of fibroblasts on unmodified and modified ATNs after 5 days of culture. Rhodamine−phalloidin staining of actin (red) and DAPI staining of nuclei (blue) of fibroblasts for examining cell adhesion and spreading patterns on ATN (A), APTMS-ATN (B), and MPTMS-ATN (C). Higher-magnification images of stained cells on ATN (D), APTMS-ATN (E), and MPTMS-ATN (F) corresponding to (A), (B), and (C). Immunostaining of ATN (G), APTMS-ATN (H), and MPTMS-ATN (I) with monoclonal antivinculin antibody (green) to rhodamine−phalloidin with DAPI-stained nuclei.

combination of angstrom-scale chemicals and nanoscale structures in APTMS- and MPTMS-modified ATNs provided better compatibility to cell growth. Therefore, APTMS and MPTMS are two alternatives to delicate biomolecules, such as proteins, because of their relatively simple composition and stable properties.

Microscopic Examination of Cell Responses to Modified Surfaces. Fibroblasts on unmodified and modified ATNs exhibited protruded filopodia based on SEM scans (Figure 4) and actin filaments in the cytoskeleton based on fluorescence images (Figure 5). Compared with the Ti web (Figure S4 in SI), all fibroblasts on unmodified (Figure 4A) and modified nanostructures (Figure 4B,C) protruded relatively more and longer filopodia and manifested more clearly a spindle phenotype.

Table 3 shows the measured length and number of filopodia of fibroblasts on the different surfaces according to the SEM images. White arrows represent where filopodia were. The average length of filopodia on ATNs (Figure 4D), APTMS-ATNs (Figure 4E), and MPTMS-ATNs (Figure 4F) were more than twice longer than those on Ti webs. It is obvious that the presence of nanostructures in ATNs led to the increased length (6.70 ± 0.56 μm) and number (26.56 ± 1.10/100 μm^2) of filopodia in cultured fibroblasts. In addition, the highest length and number of filopodia (8.18 ± 0.92 μm and 38.53 ± 1.57/100 μm^2, respectively) were observed on APTMS-ATNs. Compared with ATNs and APTMS-ATNs, MPTMS-ATNs resulted in relatively unfavorable cell attachment as shown by the shorter length and fewer filopodia (6.39 ± 0.62 μm and 26.47 ± 1.31/100 μm^2, respectively) on the nanoscale surface.

Table 3. Statistical Analyses[a] of Length and Number of Filopodia of Fibroblasts Cultured on Ti Web, ATN, APTMS-ATN, and MPTMS-ATN

	length of filopodia (μm)	number of filopodia (100 μm^{-2})
Ti web	2.72 ± 0.40	15.17 ± 0.79
ATN	6.70 ± 0.56 ([c])	26.56 ± 1.10 ([b])
APTMS-ATN	8.18 ± 0.92 ([c])	38.53 ± 1.57 ([c])
MPTMS-ATN	6.39 ± 0.62 ([c])	26.47 ± 1.31 ([b])

[a] n = 36; value = mean ± SEM. [b] $p < 0.05$. [c] $p < 0.01$, significant difference relative to Ti web.

Filopodia, typically found at the leading edge of a migrating or an elongating cell, have been associated with the ability of cells to probe chemically and topographically heterogeneous surfaces.[52] When cells contact a substrate, cells first protrude filamentous (F)-actin filopodia[52] to sense the external nanostructure environment.[10,12,19,40] A nanoscale structure with dimensions of 15 nm has been found to promote cell adhesion, extensive filopodia, proliferation, migration, and differentiation of different cell types, such as MSCs and hematopoietic stem cells, in contrast with structures with 100 nm dimensions.[7,19] Here, the increased number of filopodia on unmodified and modified ATNs, a diameter of 60 nm, implies that fibroblasts firmly anchored on the substrates. The effect of the nanoporous surface of TiO_2 on cell adhesion and proliferation has also been investigated in other studies.[7,19,25,28]

It was observed that the filopodia of fibroblasts actually propagate into the nanotubes.[51] This behavior was also observed in MC3T3-E1 osteoblast cells on aligned TiO_2 nanotubes.[53] Abundant amounts of extracellular matrix between neighboring osteoblast cells were observed on nanotubular surfaces, with filopodia extensions protruding from the cells to grasp the nanoporous surface for anchorage.[25] Furthermore, it was observed that slight changes in nanotube dimensions caused a change in osteoblast behavior: small-diameter nanotubes promoted osteoblast adhesion, while large-diameter nanotubes resulted in lower population of cells with extremely elongated cell morphology.[28]

Evaluation of cell viability and proliferation in this study revealed significantly higher cell numbers on unmodified and modified ATNs probably because of the crucial role of dynamic actin assemblies of filopodia in mitosis during cell growth.[10,52,54] Our findings also showed that appropriate small chemical modification can vary cell behavior in the nanoscale regime. For instance, fibroblasts presented longer and more extensive fibrous networks of filopodia on APTMS-ATNs with 60 nm diameter nanotubes (Figure 4 and Table 3). IUPAC defines biocompatibility as the "ability to be in contact with a living system without producing an adverse effect".[55] Supposing that cell seeding and surface modification were done uniformly on the substrate, it is possible that APTMS modification produced a more biocompatible surface for fibroblast cells according to our analyses of cell viability and proliferation.

In order to distinguish differences in fibroblast adhesion and spreading patterns on unmodified and modified ATNs, rhodamine−phalloidin and DAPI stainings were performed (Figure 5A−F). Fluorescent phalloidin is widely used in the study of actin networks in biology. In comparison with the uneven cell distribution on ATN (Figure 5A) and MPTMS-ATN (Figure 5C), cells on APTMS-ATN (Figure 5B) expressed directional growth and even spreading on the fifth day of culture based on actin−phalloidin staining. In the higher-magnification images (Figure 5D−F), APTMS-ATN (Figure 5E) shows actin distribution in the perinuclear spaces and cell edges and shows a directional and organized cell growth with elongated fibroblast phenotype. However, fibroblasts on ATNs (Figure 5D) have a morphology with disordered distribution of cells on the substrate. Fibroblasts expressed the prevalence of actin-containing stress fibers from nuclei to cell edges on MPTMS-ATNs (Figure 5F).

Supplementary immunostaining with monoclonal antivinculin antibody to rhodamine−phalloidin was performed (Figure 5G−I) to further visualize the actin-based cytoskeleton in the cell−cell and cell−substrate junctions.[14,56] Vinculin expression (green fluorescence) represents focal adhesions to the surfaces of unmodified and modified ATNs. Vinculin, which associates with the integrin-based cell−ECM interactions, can regulate traction forces and adhesion strength to the extracellular environment.[57] Previous studies indicate TiO_2 nanotubes had a diameter of 30−50 nm and showed MSCs spread out with a phenotypical morphology owing to dense clusters of integrins on the nanotubes.[7,19] The presence of integrin-associated vinculin and stress fibers in the cytoplasm of fibroblasts in unmodified and modified ATNs shows that cells anchored onto the three-dimensional (3D) environment with different morphologies. In addition, the relatively homogeneous expression of vinculin on ATNs and APTMS-ATNs (Figure 5G,H) means that fibroblasts adhered well through integrins on the substrates and possessed better cell−cell and cell−substrate interactions to promote growth. On the other hand, vinculin expression with a relatively sparse distribution around the nuclei on MPTMS-ATNs (Figure 5I) means that fibroblasts spread less and had less traction force for anchoring onto the

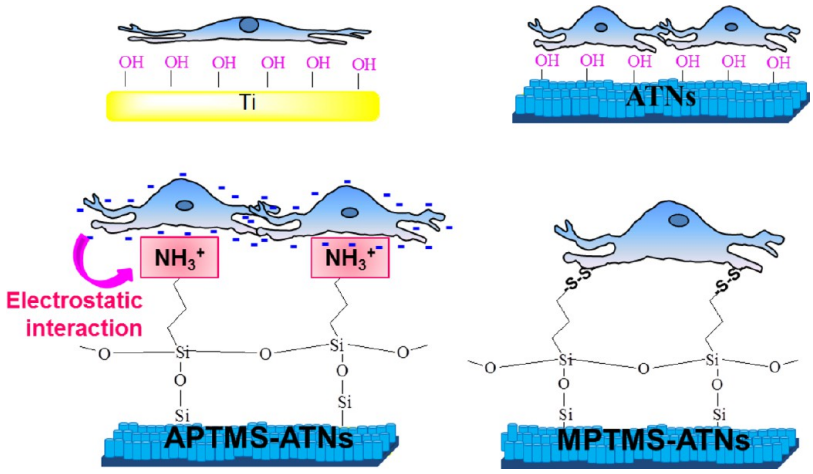

Figure 6. Schematic of the proposed mechanisms of the interfacial effects of nanostructures and small chemicals on cell attachment. The substantial increase of surface roughness of ATNs offers more contact areas for fibroblasts proliferation compared with Ti substrate. APTMS-ATNs with a positively charged surface create a suitable environment for firm attachment and flat spreading of cells via electrostatic interaction between the cell membrane and APTMS. MPTMS interacts with cells by forming new disulfide bonds with proteoglycans on the cell membrane, resulting in cells with a 3D solid shape and clear contours due to the lack of surface contact.

substrate.[57] The different cell morphology observed for MPTMS-ATNs is due to less focal adhesion of cells, resulting in concrete and solid shapes.[52,58,59] This explains the contracted and 3D solid morphology of fibroblasts on MPTMS-ATNs in the SEM scan (Figure 4F).

Mechanisms of Interfacial Interaction between Cells and Substrates. Conventional tissue culture polystyrene dishes are treated with gas plasma to create oxygen-containing groups on the surface so as to gain a negatively charged hydrophilic surface after addition of medium.[60] Oxygen-plasma-treated ATNs also increase oxygen-containing groups, such as −OH groups, and possess negatively charged hydrophilic surfaces in contact with medium. The negatively charged hydrophilic surface with highly energetic oxygen-containing groups would then evenly bind with cell adhesive proteins and render a surface for cell growth.[61] Regardless of the property of the negatively charged hydrophilic surface, our observation found that relatively higher fibroblast growth on plasma-treated ATNs (Table 2) is due to the nanostructure of ATN.

Since the cell membrane comprises a negatively charged phospholipid bilayer with embedded proteins and sugars, positively charged surfaces promote cell adhesion and guide cell growth among mammalian cells.[62] When a negative charge is imparted on surfaces, cell attachment is relatively low due to the inhibition of interactions with negatively charged cell surface proteoglycans or prevention of adsorption of negatively charged adhesive proteins, such as serum albumin, the most abundant protein in serum.[48] Figure 6 illustrates the possible mechanisms of interfacial interaction between cells and ATNs and between cells and small chemicals in this study. The growth of cell number and filopodia in ATNs, APTMS-ATNs, and MPTMS-ATNs in Table 2 and Table 3 showed the substantial increases because of surface roughness and more contact areas for fibroblast proliferation compared with Ti substrate. Studies also demonstrated that nanostructures increased the surface roughness and significantly influenced cell features and behavior, such as protrusion of filopodia and cell proliferation.[2−10,12,19,21,24−28] On the other hand, APTMS-ATN surface promoted cell attachment owing to positively charged amine functional groups.[30,48] This is supported by the relatively higher cell growth (Table 2), homogeneous vinculin expression (Figure 5H), and flat filamentous network from fibroblasts (Figure 4E) in APTMS-ATNs. On the basis of our ESCA analyses, surface modification with APTMS was shown to introduce both amine groups ($-NH_2$) and ammonium ions ($-NH_3^+$) to the surface of the ATNs (Figure 1B). Although the ammonium ions were probably due to previous exposure of the samples to water vapor, ammonium ions on the APTMS-ATN surface were probably present during cell culture as well because amine groups are easily protonated in the physiological environment. The resulting positively charged surface renders a suitable environment for firm attachment and flat spreading of fibroblast cells via electrostatic attraction.

As for cell growth on MPTMS-ATNs, Figure 6 shows a different interfacial mechanism compared with APTMS-ATNs because of the specific functional groups involved. This is supported by the contracted and 3D solid morphology of fibroblast cells on MPTMS-ATNs (Figure 4C,F), which is different from the flat morphology observed in APTMS-ATNs (Figure 4B,E). Previous studies have shown that mercapto functional groups are highly reactive and easily form new disulfide bonds with proteins through an interchange−reduction reaction.[63−65] Although mercapto group-modified silicon surfaces were shown to lead to fewer cancer cells in comparison with −COOH-, $-NH_2$-, −OH-, and $-CH_3$-modified substrates,[66] the mechanism of cell attachment or detachment on these modified substrates has not been discussed. As shown by vinculin immunostaining, cells on our MPTMS-ATNs revealed a relatively 3D solid morphology and clear contours (Figure 4) caused by the lack of focal adhesions (Figure 5I). Therefore, the mercapto groups on the MPTMS-ATNs result in a relatively unstable environment for fibroblasts, leading to cell detachment during routine cell culture. In other words, MPTMS-ATNs have essentially good biocompatibility but produce less contact area for cell attachment. On the basis of our results (Table 2), MPTMS-ATNs were shown to result in better cell proliferation than unmodified ATNs, but APTMS-ATNs showed the highest cell growth after 5 days of culture as a result of more cell−substrate contact areas for cell attachment.

Surface roughness, greater surface area, and additional functional chemicals on ATNs promote cell attachment and

proliferation. Hydrophilicity, on the other hand, is believed to have minor influence on the expression of adhesion-related molecules on the cell surface. Our results indicate that the nanoscale surface roughness of ATNs was the main cause of enhanced cell proliferation. Likewise, APTMS functional groups provided closer contact between cells and substrates, thereby promoting cell spreading, growth, and orientation (Figure 5B,E,H). Therefore, the relatively better biocompatibility of APTMS-ATNs is mainly a consequence of the synergistic interfacial effects of nanotube surface topology and positive surface charge, instead of enhanced surface hydrophilicity. For both APTMS-ATNs and MPTMS-ATNs, however, the mechanisms of interfacial effects show that specific functional groups have the capacity to alter the properties of nanoscale surfaces and affect the stability of the cell culture environment.

CONCLUSIONS

The combined interfacial effects of nanoscale architecture and small chemicals alter fibroblast cell attachment and growth. Although plasma-treated polystyrene dishes and ATNs presented the negatively charged hydrophilic surfaces for adsorbing positively charged cell adhesive proteins, the nanotubular structure of ATNs greatly enhanced cell growth. In addition, both nanotopographical structures and surface functional groups have a significant impact on the length and number of protruded filopodia from the fibroblasts. Although APTMS and MPTMS are too small to be visualized by SEM (length $\approx$ 0.8 nm), the influence of these small chemicals on cell attachment, growth, and morphology is very apparent. APTMS-modified ATNs have a positively charged surface that promotes electrostatic attraction of negatively charged cell surface proteoglycans and adsorption of negatively charged adhesive proteins. On the other hand, MPTMS-modified ATNs contain mercapto functional groups which produce less contact area for cell attachment. Consequently, the specific functional group of surface chemical modifications can alter the stability of the culture environment by making subtle changes on the properties of nanoscale structures. On the basis of our results, ATNs materials, in particular, APTMS-modified ATNs, are shown to be suitable for future application in implants where integration with the native environment is crucial.

This study provided insights into how interfacial interactions due to nanostructures and small chemical modifications affect cell fate. In the future, it will be possible to combine amine, mercapto, and other functional groups of small chemicals for selectively functionalizing substrates and patterning cells. These materials can be used for advanced medical or biological studies on cell communication and investigation of various cell behaviors, such as adhesion, migration, and differentiation.

ASSOCIATED CONTENT

Supporting Information

Characterization of ATNs using SEM and XRD, cell quantification by cell cycle analysis using MetaMorph, LIVE/DEAD *in situ* staining of overgrown fibroblasts on APTMS-ATN, and SEM images of fibroblast morphology and filopodia on Ti web. This material is available free of charge via the Internet at http://pubs.acs.org.

AUTHOR INFORMATION

Corresponding Author

*Tel: +886-4-2284-0732 (ext. 302). Fax: +886-4-2285-2422. E-mail: splin@dragon.nchu.edu.tw.

Notes

The authors declare no competing financial interest.

ACKNOWLEDGMENTS

Technical support was given by the Center of Nanoscience and Nanotechnology at National Chung Hsing University and National Nano Device Laboratories in Taiwan. The authors would like to thank Prof. Wen-Tai Chiu of the Department of Biomedical Engineering, National Cheng Kung University for useful discussions on fluorescence staining. This work was supported by the National Science Council of Taiwan under Contract Numbers NSC 100-2221-E-005-016-, NSC 101-2221-E-005-002-, NSC 101-2923-E-005-001-MY3, and NSC 102-2221-E-005-005-MY3.

REFERENCES

(1) Ventre, M.; Causa, F.; Netti, P. A. Determinants of Cell-Material Crosstalk at The Interface: towards Engineering of Cell Instructive Materials. *J. R. Soc., Interface* **2012**, *9*, 2017−2032.

(2) Bucaro, M. A.; Vasquez, Y.; Hatton, B. D.; Aizenberg, J. Fine-Tuning The Degree of Stem Cell Polarization and Alignment on Ordered Arrays of High-Aspect-Ratio Nanopillars. *ACS Nano* **2012**, *6*, 6222−6230.

(3) Tatkiewicz, W. I.; Seras-Franzoso, J.; Garcia-Fruitos, E.; Vazquez, E.; Ventosa, N.; Peebo, K.; Ratera, I.; Villaverde, A.; Veciana, J. Two-Dimensional Microscale Engineering of Protein-Based Nanoparticles for Cell Guidance. *ACS Nano* **2013**, *7*, 4774−4784.

(4) Lim, J. Y.; Donahue, H. J. Cell Sensing and Response to Micro- and Nanostructured Surfaces Produced by Chemical and Topographic Patterning. *Tissue Eng.* **2007**, *13*, 1879−1891.

(5) Koegler, P.; Clayton, A.; Thissen, H.; Santos, G. N. C.; Kingshott, P. The Influence of Nanostructured Materials on Biointerfacial Interactions. *Adv. Drug Delivery Rev.* **2012**, *64*, 1820−1839.

(6) Gumusderelioglu, M.; Kaya, F. B.; Beskardes, I. G. Comparison of Epithelial and Fibroblastic Cell Behavior on Nano/Micro-Topographic PCL Membranes Produced by Crystallinity Control. *J. Colloid Interface Sci.* **2011**, *358*, 444−453.

(7) Park, J.; Bauer, S.; von der Mark, K.; Schmuki, P. Nanosize and Vitality: TiO_2 Nanotube Diameter Directs Cell Fate. *Nano Lett.* **2007**, *7*, 1686−1691.

(8) Li, X.; Gao, H.; Uo, M.; Sato, Y.; Akasaka, T.; Feng, Q.; Cui, F.; Liu, X.; Watari, F. Effect of Carbon Nanotubes on Cellular Functions In Vitro. *J. Biomed. Mater. Res., Part A* **2009**, *91A*, 132−139.

(9) Kubo, K.; Tsukimura, N.; Iwasa, F.; Ueno, T.; Saruwatari, L.; Aita, H.; Chiou, W. A.; Ogawa, T. Cellular Behavior on TiO_2 Nanonodular Structures in a Micro-to-Nanoscale Hierarchy Model. *Biomaterials* **2009**, *30*, 5319−5329.

(10) Hamilton, D. W.; Oates, C. J.; Hasanzadeh, A.; Mittler, S. Migration of Periodontal Ligament Fibroblasts on Nanometric Topographical Patterns: Influence of Filopodia and Focal Adhesions on Contact Guidance. *PLoS One* **2010**, *5*, e15129.

(11) Dalby, M. J.; Gadegaard, N.; Riehle, M. O.; Wilkinson, C. D. W.; Curtis, A. S. G. Investigating Filopodia Sensing Using Arrays of Defined Nano-Pits Down to 35 nm Diameter in Size. *Int. J. Biochem. Cell Biol.* **2004**, *36*, 2005−2015.

(12) Albuschies, J.; Vogel, V. The Role of Filopodia in The Recognition of Nanotopographies. *Sci. Rep.* **2013**, *3*, 1658.

(13) Jiang, K.; Fan, D.; Belabassi, Y.; Akkaraju, G.; Montchamp, J. L.; Coffer, J. L. Medicinal Surface Modification of Silicon Nanowires: Impact on Calcification and Stromal Cell Proliferation. *ACS Appl. Mater. Interfaces* **2009**, *1*, 266−269.

(14) Ryoo, S. R.; Kim, Y. K.; Kim, M. H.; Min, D. H. Behaviors of NIH-3T3 Fibroblasts on Graphene/Carbon Nanotubes: Proliferation, Focal Adhesion, and Gene Transfection Studies. *ACS Nano* **2010**, *4*, 6587−6598.
(15) Hori, N.; Iwasa, F.; Ueno, T.; Takeuchi, K.; Tsukimura, N.; Yamada, M.; Hattori, M.; Yamamoto, A.; Ogawa, T. Selective Cell Affinity of Biomimetic Micro-Nano-Hybrid Structured TiO_2 Overcomes The Biological Dilemma of Osteoblasts. *Dent. Mater.* **2010**, *26*, 275−287.
(16) Chen, L.; McCrate, J. M.; Lee, J. C.; Li, H. The Role of Surface Charge on The Uptake and Biocompatibility of Hydroxyapatite Nanoparticles with Osteoblast Cells. *Nanotechnology* **2011**, *22*, 105708.
(17) Dalby, M. J.; Yarwood, S. J.; Riehle, M. O.; Johnstone, H. J. H.; Affrossman, S.; Curtsi, A. S. G. Increasing Fibroblast Response to Materials Using Nanotopography: Morphological and Genetic Measurements of Cell Response to 13-nm-High Polymer Demixed Islands. *Exp. Cell Res.* **2002**, *276*, 1−9.
(18) Dalby, M. J.; Giannaras, D.; Riehle, M. O.; Gadegaard, N.; Affrossman, S.; Curtis, A. S. G. Rapid Fibroblast adhesion to 27 nm High Polymer Demixed Nano-Topography. *Biomaterials* **2004**, *25*, 77−83.
(19) Park, J.; Bauer, S.; Schlegel, K. A.; Neukam, F. W.; von der Mark, K.; Schmuki, P. TiO_2 Nanotube Surfaces: 15 nm - An Optimal Length Scale of Surface Topography for Cell Adhesion and Differentiation. *Small* **2009**, *5*, 666−671.
(20) Sjostrom, T.; Dalby, M. J.; Hart, A.; Tare, R.; Oreffo, R. O. C.; Su, B. Fabrication of Pillar-Like Titania Nanostructures on Titanium and Their Interactions with Human Skeletal Stem Cells. *Acta Biomater.* **2009**, *5*, 1433−1441.
(21) Variola, F.; Brunski, J. B.; Orsini, G.; de Oliveira, P. T.; Wazen, R.; Nanci, A. Nanoscale Surface Modifications of Medically Relevant Metals: State-of-The Art and Perspectives. *Nanoscale* **2011**, *3*, 335−353.
(22) Ingham, C. J.; ter Maat, J.; de Vos, W. M. Where Bio Meets Nano: The Many Uses for Nanoporous Aluminum Oxide in Biotechnology. *Biotechnol. Adv.* **2012**, *30*, 1089−1099.
(23) Shankar, K.; Mor, G. K.; Prakasam, H. E.; Yoriya, S.; Paulose, M.; Varghese, O. K.; Grimes, C. A. Highly-Ordered TiO_2 Nanotube Arrays up to 220 μm in Length: Use in Water Photoelectrolysis and Dye-Sensitized Solar Cells. *Nanotechnology* **2007**, *18*, 065707.
(24) Peng, L.; Eltgroth, M. L.; LaTempa, T. J.; Grimes, C. A.; Desai, T. A. The Effect of TiO_2 Nanotubes on Endothelial Function and Smooth Muscle Proliferation. *Biomaterials* **2009**, *30*, 1268−1272.
(25) Das, K.; Bose, S.; Bandyopadhyay, A. TiO_2 Nanotubes on Ti: Influence of Nanoscale Morphology on Bone Cell−Materials Interaction. *J. Biomed. Mater. Res., Part A* **2009**, *90A*, 225−237.
(26) Brammer, K. S.; Oh, S.; Gallagher, J. O.; Jin, S. Enhanced Cellular Mobility Guided by TiO_2 Nanotube Surfaces. *Nano Lett.* **2008**, *8*, 786−793.
(27) Depan, D.; Misra, R. D. K. The Interplay between Nanostructured Carbon-Grafted Chitosan Scaffolds and Protein Adsorption on The Cellular Response of Osteoblasts: Structure-Function Property Relationship. *Acta Biomater.* **2013**, *9*, 6084−6094.
(28) Brammer, K. S.; Oh, S.; Cobb, C. J.; Bjursten, L. M.; Heyde, H. v. d.; Jin, S. Improved Bone-Forming Functionality on Diameter-Controlled TiO_2 Nanotube Surface. *Acta Biomater.* **2009**, *5*, 3215−3223.
(29) Beamson, G.; Briggs, D. High-Resolution Monochromated X-Ray Photoelectron-Spectroscopy of Organic Polymers - a Comparison between Solid-State Data for Organic Polymers and Gas-Phase Data for Small Molecules. *Mol. Phys.* **1992**, *76*, 919−936.
(30) Liao, J. D.; Lin, S. P.; Wu, Y. T. Dual Properties of The Deacetylated Sites in Chitosan for Molecular Immobilization and Biofunctional Effects. *Biomacromolecules* **2005**, *6*, 392−399.
(31) Crist, B. V. *Handbook of Monochromatic XPS Spectra The Elements and Native Oxides*; Wiley: Chichester, 2000.
(32) Beamson, G.; Briggs, D. *High Resolution XPS of Organic Polymers The Scienta ESCA300 Database*; Wiley: Chichester, 1992.
(33) Mor, G. K.; Varghese, O. K.; Paulose, M.; Shankar, K.; Grimes, C. A. A Review on Highly Ordered, Vertically Oriented TiO_2 Nanotube Arrays: Fabrication, Material Properties, and Solar Energy Applications. *Sol. Energy Mater. Sol. Cells* **2006**, *90*, 2011−2075.
(34) Ma, Q.; Wang, W.; Chu, P. K.; Mei, S.; Ji, K.; Jin, L.; Zhang, Y. Concentration- and Time-Dependent Response of Human Gingival Fibroblasts to Fibroblast Growth Factor 2 Immobilized on Titanium Dental Implants. *Int. J. Nanomed.* **2012**, *7*, 1965−1976.
(35) Gittens, R. A.; McLachlan, T.; Olivares-Navarrete, R.; Cai, Y.; Berner, S.; Tannenbaum, R.; Schwartz, Z.; Sandhage, K. H.; Boyan, B. D. The Effects of Combined Micron-/Submicron-Scale Surface Roughness and Nanoscale Features on Cell Proliferation and Differentiation. *Biomaterials* **2011**, *32*, 3395−3403.
(36) Vega, V.; Prida, V. M.; Hernandez-Velez, M.; Manova, E.; Aranda, P.; Ruiz-Hitzky, E.; Vazquez, M. Influence of Anodic Conditions on Self-Ordered Growth of Highly Aligned Titanium Oxide Nanopores. *Nanoscale Res. Lett.* **2007**, *2*, 355−363.
(37) Xiao, X. F.; Ouyang, K. G.; Liu, R. F.; Liang, J. H. Anatase Type Titania Nanotube Arrays Direct Fabricated by Anodization without Annealing. *Appl. Surf. Sci.* **2009**, *255*, 3659−3663.
(38) Everett, E. T. Fluoride's Effects on The Formation of Teeth and Bones, and The Influence of Genetics. *J. Dent. Res.* **2011**, *90*, 552−560.
(39) Förch, R.; Schönherr, H.; Jenkins, A. T. A. In *Surface Design: Applications in Bioscience and Nanotechnology*; Wiley-VCH: Weinheim, 2009; Appendix C, pp 471−473.
(40) Kashima, D. P.; Whangdee, P.; Chukasorn, S.; Srimaneepong, V.; Watanabe, T. Effects of Surface Roughness and Chemical Species on Hydrophilicity of Anodized Film on Ti-6Al-4V Formed at a Low Current Density. *Adv. Mater. Res.* **2013**, *664*, 774−779.
(41) Chu, P. K.; Chen, J. Y.; Wang, L. P.; Huang, N. Plasma-Surface Modification of Biomaterials. *Mater. Sci. Eng., R* **2002**, *36*, 143−206.
(42) Liu, X.; Chu, P. K.; Ding, C. Surface Modification of Titanium, Titanium Alloys, and Related Materials for Biomedical Applications. *Mater. Sci. Eng., R* **2004**, *47*, 49−121.
(43) Israelachvili, J. N. *Intermolecular and Surface Forces*, 3rd ed; Academic Press: Burlington MA, 2011.
(44) Szyszka, D. Study of Contact Angle of Liquid on Solid Surface and Solid on Liquid Surface. *Pr. Nauk. Inst. Gorn. Politech. Wroclaw.* **2012**, 131−146.
(45) Biazar, E.; Heidari, M.; Asefnejad, A.; Montazeri, N. The Relationship between Cellular Adhesion and Surface Roughness in Polystyrene Modified by Microwave Plasma Radiation. *Int. J. Nanomed.* **2011**, *6*, 631−639.
(46) Van der Valk, P.; Van Pelt, A.; Busscher, H.; De Jong, H.; Wildevuur, C. R.; Arends, J. Interaction of Fibroblasts and Polymer Surfaces: Relationship between Surface Free Energy and Fibroblast Spreading. *J. Biomed. Mater. Res.* **1983**, *17*, 807−817.
(47) Schakenraad, J.; Busscher, H.; Wildevuur, C. R.; Arends, J. The Influence of Substratum Surface Free Energy on Growth and Spreading of Human Fibroblasts in The Presence and Absence of Serum Proteins. *J. Biomed. Mater. Res.* **1986**, *20*, 773−784.
(48) Webb, K.; Hlady, V.; Tresco, P. A. Relative Importance of Surface Wettability and Charged Functional Groups on NIH 3T3 Fibroblast Attachment, Spreading, and Cytoskeletal Organization. *J. Biomed. Mater. Res.* **1998**, *41*, 422−430.
(49) Popat, K. C.; Leoni, L.; Grimes, C. A.; Desai, T. A. Influence of Engineered Titania Nanotubular Surfaces on Bone Cells. *Biomaterials* **2007**, *28*, 3188−3197.
(50) Popat, K. C.; Eltgroth, M.; LaTempa, T. J.; Grimes, C. A.; Desai, T. A. Decreased Staphylococcus Epidermis Adhesion and Increased Osteoblast Functionality on Antibiotic-Loaded Titania Nanotubes. *Biomaterials* **2007**, *28*, 4880−4888.
(51) Hazan, R.; Sreekantan, S.; Khalil, A. A.; Nordin, I.; Mat, I. Surface Engineering of Titania for Excellent Fibroblast 3T3 Cell-Metal Interaction. *J. Phys. Sci.* **2009**, *20*, 35−47.
(52) Mattila, P. K.; Lappalainen, P. Filopodia: Molecular Architecture and Cellular Functions. *Nat. Rev. Mol. Cell Biol.* **2008**, *9*, 446−454.

(53) Oh, S.; Daraio, C.; Chen, L. H.; Pisanic, T. R.; Finones, R. R.; Jin, S. Significantly Accelerated Osteoblast Cell Growth on Aligned TiO_2 Nanotubes. *J. Biomed. Mater. Res., Part A* **2006**, *78*, 97−103.
(54) Holt, B. D.; Short, P. A.; Rape, A. D.; Wang, Y. L.; Islam, M. F.; Dahl, K. N. Carbon Nanotubes Reorganize Actin Structures in Cells and ex Vivo. *ACS Nano* **2010**, *4*, 4872−4878.
(55) Vert, M.; Hellwich, K.-H.; Hess, M.; Hodge, P.; Kubisa, P.; Rinaudo, M.; Schué, F. Terminology for Biorelated Polymers and Applications (IUPAC Recommendations 2012). *Pure Appl. Chem.* **2012**, *84*, 377−410.
(56) Dolatshahi-Pirouz, A.; Jensen, T.; Kraft, D. C.; Foss, M.; Kingshott, P.; Hansen, J. L.; Larsen, A. N.; Chevallier, J.; Besenbacher, F. Fibronectin Adsorption, Cell Adhesion, and Proliferation on Nanostructured Tantalum Surfaces. *ACS Nano* **2010**, *4*, 2874−2882.
(57) Dumbauld, D. W.; Lee, T. T.; Singh, A.; Scrimgeour, J.; Gersbach, C. A.; Zamir, E. A.; Fu, J.; Chen, C. S.; Curtis, J. E.; Craig, S. W.; García, A. J. How Vinculin Regulates Force Transmission. *Proc. Natl. Acad. Sci. U.S.A.* **2013**, *110*, 9788−9793.
(58) Yeung, T.; Georges, P. C.; Flanagan, L. A.; Marg, B.; Ortiz, M.; Funaki, M.; Zahir, N.; Ming, W.; Weaver, V.; Janmey, P. A. Effects of Substrate Stiffness on Cell Morphology, Cytoskeletal Structure, and Adhesion. *Cell Motil. Cytoskeleton* **2005**, *60*, 24−34.
(59) Pellegrin, S.; Mellor, H. Actin Stress Fibres. *J. Cell Sci.* **2007**, *120*, 3491−3499.
(60) Ramsey, W. S.; Hertl, W.; Nowlan, E. D.; Binkowski, N. J. Surface Treatments and Cell Attachment. *In Vitro* **1984**, *20*, 802−808.
(61) Shen, M.; Horbett, T. A. The Effects of Surface Chemistry and Adsorbed Proteins on Monocyte/Macrophage Adhesion to Chemically Modified Polystyrene Surfaces. *J. Biomed. Mater. Res.* **2001**, *57*, 336−345.
(62) Healy, K. E.; Lom, B.; Hockberger, P. E. Spatial Distribution of Mammalian Cells Dictated by Material Surface Chemistry. *Biotechnol. Bioeng.* **1994**, *43*, 792−800.
(63) Mosher, D. F.; Fogerty, F. J.; Chernousov, M. A.; Barry, E. L. R. Assembly of Fibronectin into Extracellular Matrix. *Ann. N.Y. Acad. Sci.* **1991**, *614*, 167−180.
(64) Bulleid, N. J.; Ellgaard, L. Multiple Ways to Make Disulfides. *Trends Biochem. Sci.* **2011**, *36*, 485−492.
(65) Castner, D. G.; Hinds, K.; Grainger, D. W. X-Ray Photoelectron Spectroscopy Sulfur 2p Study of Organic Thiol and Disulfide Binding Interactions with Gold Surfaces. *Langmuir* **1996**, *12*, 5083−5086.
(66) Xu, S.-J.; Cui, F.-Z.; Yu, X.-L.; Kong, X.-D. Glioma Cell Line Proliferation Controlled by Different Chemical Functional Groups *in Vitro*. *Front. Mater. Sci.* **2013**, *7*, 69−75.